Small Angle Neutron Scattering Studies on Block Copolymer Micelles with Varying Core-Solvent Interactions

A Thesis

Presented to

the Faculty of the Department of Chemical and Biomolecular Engineering

University of Houston

In Partial Fulfillment

of the Requirements of the Degree

Master of Science

in Chemical Engineering

by

Tyler Cooksey

May 2016

Small Angle Neutron Scattering Studies on Block Copolymer Micelles with Varying Core-Solvent Interactions

Tyler Cooksey

Approved:

Chair of the Committee
Megan L. Robertson, Assistant Professor
Chemical and Biomolecular Engineering

Committee Members:

Jacinta C. Conrad, Assistant Professor
Chemical and Biomolecular Engineering

Paul Ruchhoeft, Associate Professor
Electrical and Computer Engineering

Suresh K. Khator, Associate Dean
Cullen College of Engineering

Michael P. Harold, Professor and Chair
Chemical and Biomolecular Engineering

Acknowledgments

To my parents, for all that they've done and given up to bring me to this point in my life and in my education,

To my grandparents, for the constant support, through the best and the worst times,

To my sister, who taught me how to learn, even before I ever wanted to, who taught me to pursue what makes me happiest.

To Dr. Megan Robertson, for this amazing opportunity and for her mentoring, pushing me to try and try again through all the trials,

To my fellow group members, Brian Rohde, Vivek Yadav, Wenyue Ding, and Guozhen Yang, for making every day a learning experience, and for the laughs and support,

To everyone I've worked with on this project, for their patience and teachings as I've stumbled along,

To Avantika Singh, for her efforts in synthesizing and characterizing materials used in this study.

To Dr. Kane Jennings, Dr. Paul Laibinis, and Dr. Peggy Bertrand, for pushing me in thinking about science beyond the classroom,

To my friends, near and far, who put up with me on a day-to-day basis, and who walk with me every step of the way,

From the bottom of my heart, I thank you all for everything.

Small Angle Neutron Scattering Studies on Block Copolymer Micelles with Varying Core-Solvent Interactions

An Abstract

of

Thesis

Presented to

the Faculty of the Department of Chemical and Biomolecular Engineering

University of Houston

In Partial Fulfillment

of the Requirements for the Degree

Master of Science

in Chemical Engineering

by

Tyler Cooksey

May 2016

Abstract

Diblock copolymers are amphiphilic molecules, which spontaneously form micelles in a selective solvent. Through careful selection of polymer composition, solvent, temperature, and pH, the physical characteristics of the micelles can be tuned, providing advantages over low molecular weight surfactants. The self-assembly of micelles in aqueous solvents has great potential in drug delivery and catalyst applications. Understanding how the properties of block copolymer micelles vary in different solvent systems is one step to utilizing the loading capabilities of the micelles in applications.

In the present study, two different molecular weight series of diblock copolymers, consisting of a hydrophobic polycaprolactone block and a hydrophilic poly(ethylene oxide) block, were introduced to a solvent mixture of deuterated tetrahydrofuran and deuterated water. The structural properties of the micelles were probed using dynamic light scattering and small angle neutron scattering, as the ratio of THF_{d8} to D_2O in the micelle solutions varied.

Table of Contents

Table of Contents (continued)

List of Figures

List of Figures (continued)

List of Tables

Chapter 1

Introduction

Amphiphilic block copolymer micelles have gained significant attention for their potential therapeutic and industrial applications (such as drug delivery and oil recovery),[1-3] and for their potential to act as easily tunable surfactants and emulsions.[4,5] Block copolymers are formed by covalently linking individual polymer chains, which can have any range of molecular weights, compositions, and properties.[6-9] By dissolving block copolymers in a solvent that is a good solvent for one block (i.e. the polymer is soluble in the solvent), but a poor solvent for the other (i.e. the polymer is immiscible with the solvent), the block copolymers spontaneously self-assemble into micelle structures. [10-12]

Block copolymer micelles form differing morphologies (e.g., spherical micelles, cylindrical micelles, and vesicles), depending on the solution and polymer characteristics. Factors that directly affect the micelle properties relate to the choice of polymer, environmental conditions, and choice of solvent. With regards to the polymer, important variables include the molecular weight of each block, the volume fraction of each block in the block copolymer, and the choice of polymer for each block.[6,7] Adjusting the temperature, pH, or addition of salts or other surfactants will also alter the micelle form.[5,13]

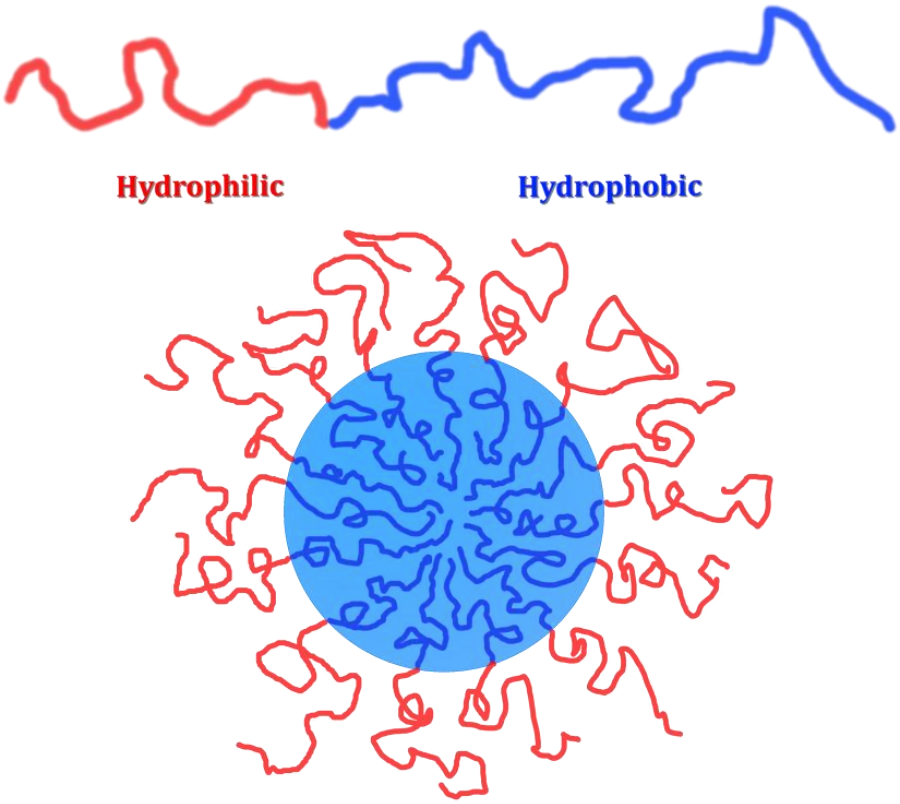

Figure 1.1 Cartoon of a block copolymer and a micelle with a homogeneous spherical core and random Gaussian chains forming the corona.

A critical factor impacting the block copolymer micelle morphology is the choice of solvent.[1,9,18] When the micelles self-assemble in solution, the equilibrium structure is obtained by the minimization of free energy.[11] One block of the copolymer has less favorable interactions with the solvent as compared to the other block, and in order to decrease the interfacial free energy, it minimizes contact with the solvent. A change in the solvent content results in a change in the interfacial free energy. Chain stretching in the core and corona occurs due to interactions between the polymer and solvent, which increases the free energy of micellization. Aggregation number and core size increase in response to the chain stretching, to

decrease the interfacial energy associated with the corona chains.[11] Hence, a balance of all these properties results in the tuning of the polymer micelle architecture.

1.1 Tuning Micelle Architecture Through Variation of Polymer-Solvent Interactions

Through careful selection of solvent quality, and thus the interactions between the solvent and the core-forming block, the interfacial free energy can be raised and lowered as desired to adjust the micelle structure and size. A number of groups have studied this previously, while varying the choice of block copolymer, molecular weight, and solvent.

The polymer identity and composition are commonly varied parameters, with prior studies employing different combinations of polymers, such as poly(ethylene oxide) (PEO),[10,12,14] poly(ε-caprolactone) (PCL), poly(propylene oxide),[10,14,15] poly(ethylene-*co*-propylene),[11] and polystyrene,[13] among others.[16] In many cases, biocompatible systems have been explored.[3] Tuning of the polymer identity and characteristics allows flexibility in manipulating the polymer-solvent interactions. Through changing the block molecular weights and ratio, it was noted that it was possible to force the polymer to become completely soluble or completely insoluble for the chosen solvent.[7] If the block ratio was held constant, the micelle size increased linearly with increasing polymer molecular weight, and the ratio of the core radius to corona thickness was constant.[4]

Varying the composition of a solvent mixture is a powerful means of tuning the polymer-solvent interactions in micelle systems. Increasing the concentration of

a less polar co-solvent (such as formamide, THF, or dimethylformamide) in water resulted in a decrease in the enthalpy and entropy of micellization, and increase in the solvation of the micelle core and corona.[8,9,11,12,15] As such, smaller micelles preferentially formed at higher solvent content.[12,15] In one case, the choice of solvent ratio caused a 36% decrease in the size of the corona by changing from a pure water system to a 40% DMF-to-water ratio, and there was no effect of the solvent ratio on the radius of gyration of the corona block, R_g.[11] Finally, the core-corona interfacial region was observed to broaden with the addition of a co-solvent, resulting in the presence of free unimers in the solution.[12]

1.2 Objectives

Moving towards the eventual goal of drug delivery systems, full knowledge of the ability to tune a specific amphiphilic block copolymer micelle assembly is needed. For that purpose, the micelle system studied here is a diblock copolymer of poly(ethylene oxide-*b*-*ε*-caprolactone) (PEO-PCL) in deuterated water (D_2O) and deuterated tetrahydrofuran (THF_{d8}) mixtures. Both poly(ethylene oxide) (PEO) and polycaprolactone (PCL) are biocompatible and partially biodegradable polymers. PEO is hydrophilic and forms the corona, while PCL is more hydrophobic and prefers to form the core of the micelles. However, solvent penetration into the core may cause solvent shielding, and both water and THF have the potential for swelling the core.[10,12]

Our goal is to firmly understand the effects of solvent composition and polymer molecular weight on the self-assembly of this micelle system. We

hypothesize that THF_{d8}, a good solvent for both blocks, will decrease the core-corona interfacial tension. We will investigate the effect of the THF_{d8} content on numerous structural properties of the micelles, such as aggregation number, core radius, and degree of core swelling due to solvent penetration.

Chapter 2

Experimental Methods

2.1 Diblock Copolymer Synthesis

All chemicals were purchased from Sigma-Aldrich unless otherwise specified. *ε*-caprolactone monomer (*ε*-CL, 97%) and benzene (ACS grade, ≥99%) were purified twice through distillation over calcium hydride (CaH_2, ACS reagent, ≥95%). Monomethoxy-polyethylene oxide (PEO) was used as received from Polymer Source. 1,5,7-triazabicyclo[4.4.0]dec-5-ene (TBD, 98%), a catalyst, was stored in a nitrogen environment to prevent deactivation and later used as received.

Poly(ethylene oxide-*b*-*ε*-caprolactone) (PEO-PCL) diblock copolymers were synthesized using monomethoxy-PEO as a macroinitiator for the ring-opening polymerization of *ε*-CL, as described in the literature.[17,18] *ε*-CL (0.24 g/mL) was added to a solution of TBD (0.072295 g catalyst/g *ε*-CL) and PEO (determined by target molecular weight ratio) in benzene. The reaction was then quenched with benzoic acid (≥99.5%). The polymer was then dissolved in tetrahydrofuran (THF, inhibitor free, chromatography grade, ≥99.5%) before precipitating in hexanes (ACS grade, >99%) and drying under vacuum, first overnight at room temperature, and then at 60°C for eight hours.

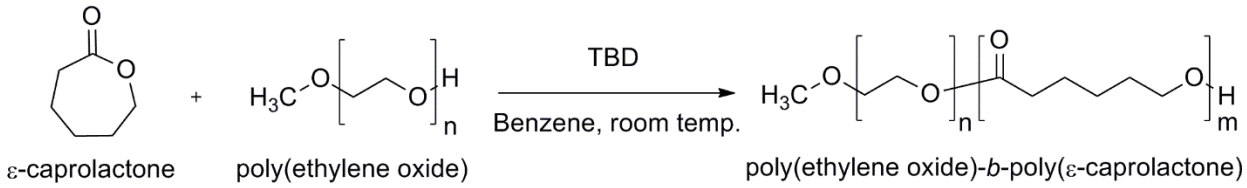

Figure 2.1 PEO-PCL synthesis schematic.

Proton nuclear magnetic resonance (^{1}H-NMR) experiments were performed on JEOL ECX-400P and ECA-500 instruments. Deuterated chloroform (99.8 atom% D) was used to dissolve the polymers. With the NMR, the relative weight fractions of the PEO and PCL blocks and the number-average molecular weight (M_n) of the PCL were determined. The presence of any residual benzene was also checked. The PEO, PCL, and ε-CL peaks were identified at 3.64, 4.05, and 4.22 ppm respectively, and the % conversion of ε-CL could be determined via peak integration.

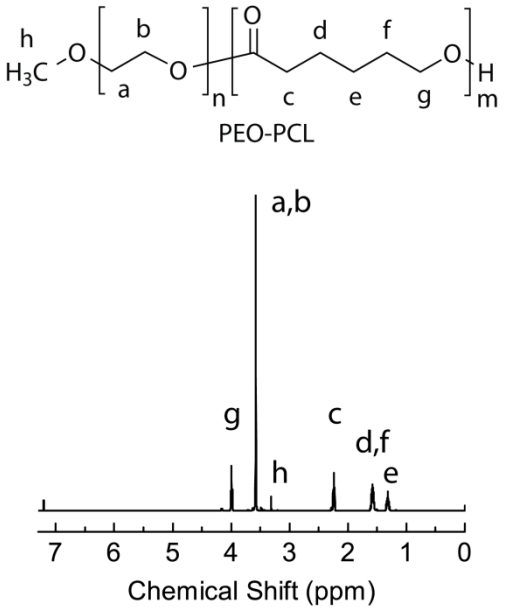

Figure 2.2 NMR spectrum for PEO_{2k}-PCL_{3k} block copolymer.

The molecular weight distribution and dispersity ($Đ$) was characterized with a Viscotek gel permeation chromatography (GPC) GPCmax instrument. THF (OmniSolv, HPLC grade) was used as the mobile phase at 30°C through Agilent ResiPore columns. Universal analysis was used to determine $Đ$. The characteristics of PEO (as purchased from Polymer Source) were determined as follows: (a) M_n = 1.9 kg/mol, $Đ$ = 1.05 and (b) M_n = 5.0 kg/mol, $Đ$ = 1.06. These numbers were used in combination with the NMR data to attain the following characteristics of the block copolymers listed in Table 1.1.

Table 1.1 Characteristics of the PEO-PCL Block Copolymers

Polymer Name	**M_n PEO (kg/mol)**	**M_n PCL (kg/mol)**	***Đ***	**PCL wt%**	**Micelle Series Containing This Polymer**
PEO_{2k}-PCL_{3k}	1.9	2.9	1.13	60	C Series (C10 to C60)
PEO_{5k}-PCL_{8k}	5.0	7.5	1.18	60	D Series (D10 to D60)

2.2 Micelle Preparation

Inhibitor-free THF (J.T. Baker, low water, HPLC grade) was purified through a solvent purification column (Pure Process Technology). Water (H_2O) was first purified using a Millipore Milli-Q Gradient water purification system to meet ASTM Type 1 Standards for reagent grade water. Fully deuterated solvents (D_2O, 99.9 atom% D; THF_{d8}, 99.5 atom% D) were used as received. Identical procedures were used for both deuterated and non-deuterated solvents at each step.

For each experiment, the THF/water ratio was varied while keeping the concentration of polymer in solvent at 1 wt%. To ensure dissolution, THF was added to a known mass of the desired diblock copolymer and left overnight. The vials were sealed with polytetrafluoroethylene (PTFE) tape to minimize solvent loss. Water was then slowly (8 mL/hour) added dropwise via syringe pump (Fisher Scientific 78-01001) over a stir plate. Afterwards, the micelle solutions were sonicated (VWR Symphony, 35 kHz) for an hour at room temperature and filtered through a 0.45 μm Nylon syringe filter (purchased from VWR) prior to analysis. The C series micelles contained PEO_{2k}-PCL_{3k} and the D series micelles contained PEO_{5k}-PCL_{8k}. The micelle nomenclature is as follows in this thesis: CXY and DXY indicate C and D series micelles with XY % THF_{d8} in the solvent (i.e. C10 and D10 both contain 10% THF_{d8} in the bulk solvent).

2.3 Dynamic Light Scattering (DLS)

DLS experiments were done using a Brookhaven Instruments BI-200SM Research Goniometer System, and then analyzed using the method of cumulants to determine the average diffusion coefficient and hydrodynamic radius. The system used a 637 nm, 30 mW laser with a 400 micron aperture at a 90° laser-detector angle, with data being collected at 25°C. Six measurements of the correlation function were taken for two minutes each, then averaged out and normalized prior to analysis, which is covered in Chapter 3. The DLS was also used to ensure the micelle samples lacked aggregation.

The hydrodynamic radius of the diffusing particles were calculated using the Stokes-Einstein relation

$$R_h = \frac{k_B T}{6\pi\eta D}, \tag{2.1}$$

where D, k_B, T, and η are the diffusion coefficient of the micelles, Boltzmann's constant, temperature, and viscosity of the solution, respectively. The solution viscosities (of THF_{d8}/D_2O mixtures) were obtained from literature values for water / tetrahydrofuran mixtures.[19]

2.4 Small-Angle Neutron Scattering (SANS)

SANS experiments were carried out at the High Flux Isotope Reactor (HFIR) at Oak Ridge National Laboratory on the CG-2 beam line. The data were collected using an incident beam wavelength of 4.72 Å. The scattering vector (q) range was 0.0028 to 0.533 Å with two different sample-to-detector distances, 1.7 and 18.5 m. Reduction of the collected data was done using the Spice IGOR Pro (WaveMetrics) routines to account for effects from sample transmission, empty Hellma cell scattering, background scattering, and detector efficiency.[20] Reduced data was then fit in SASView using a micelle form factor model by Pedersen et al.,[10,21] which is covered in Section 3.2.

Chapter 3

Micelle Structure Modeling

3.1 DLS and the Method of Cumulants

Dynamic light scattering is a commonly used technique for measuring the distribution of sizes of particles or polymers in a solution on a micro- to nano-scale.[22] By studying how light of a known wavelength scatters from interacting with the particles, the hydrodynamic radius and diffusion coefficient can be calculated.[23] At short decay times, the location of micelles in solution are correlated with their position previously, as the micelles have not had time to diffuse significantly.[24] At longer time scales though, any given micelle can have diffused to an entirely different location, and therefore the locations are no longer correlated. Analyzing the scattering intensity and how it changes due to this motion over short and long time leads to an autocorrelation function.

$$g^2(q;\tau) = \frac{\langle I(t) * I(t+\tau)\rangle}{\langle I(t)\rangle^2} \tag{3.1}$$

is the second-order correlation function. $g^2(q;\tau)$ is measured with a goniometer, and it relates intensity of scattering $I(t)$ to various decay times τ.

$$g^2(q;\tau) = 1 + \beta[g^1(q;\tau)]^2 \tag{3.2}$$

defines the Siegert relation, which states that this second-order correlation function (g^2) can be calculated as a function of the first-order correlation function

$$g^1(q;\tau) = \exp(-\Gamma\tau) \text{ (in monodisperse systems)} \tag{3.3}$$

$$\text{or } g^1(q;\tau) = \int_0^\infty \mathrm{G}(\Gamma)\exp(-\Gamma\tau)d\Gamma \text{ (in polydisperse systems),} \tag{3.4}$$

$$\text{where } \Gamma = Dq^2, \text{and} \tag{3.5}$$

$$q = \frac{4\pi n_o}{\lambda}\sin\left(\frac{\theta}{2}\right). \tag{3.6}$$

The Siegert relation holds when there are an adequate number of scatterers and these scatterers do not have restricted motion. In the method of cumulants, the first-order function (g^1) is fit to the data, and then translated back into the second-order function.

$G(\Gamma)$ is the distribution of the decay rates in polydisperse samples.[22,25,26] Since the scattering vector q is a function of known parameters (the laser-detector angle θ, the solution refractive index n_0, and laser wavelength λ) the equation for Γ (Eq. 3.5) can yield D by minimizing the differences between g^2 of the data and g^2 of the fit. Once D is calculated, R_h is calculated using the Stokes-Einstein relation (Eq. 1).

3.2 SANS and Micelle Model Fitting

Small angle neutron scattering (SANS) is a technique for probing nanoscale structure.[27] Neutrons of a known wavelength, produced either via nuclear fission or spallation of a high molecular weight nucleus, are directed at the sample and the resulting scattered intensity as a function of scattering angle is measured. The elastic scattering of these neutrons with the nuclei of the sample can be described using the scattering length. As a result, deuteration of samples is a powerful

labeling method, since hydrogen and deuterium scatter neutrons differently, and therefore provide contrast in SANS.

In a two-component suspension of non-overlapping objects (such as spheres in solution), there are two major contributors to the coherent scattering intensity: the form factor *P(q)* (the scattering interference within a single object) and the structure factor *S(q)* (the scattering interference between distinct objects).[28] The combination of these two, scaled by the contrast ($\Delta\rho$) and number of scattering objects n_p and their volume *V*, gives the coherent scattering intensity $I_{coherent}(q)$ as

$$I_{coherent}(q) = n_p \Delta\rho^2 V^2 P(q) S(q). \quad (3.7)$$

In the micelle system discussed in this thesis, the differences in the scattering lengths of the components in the mixture are incorporated into *P(q)*, and is described in the following section (Section 3.2.1). In dilute systems, such as the micelles studied here, *S(q)* is taken to be one. The scattering lengths of each component in the system are listed in Table 3.1.

Table 3.1 Scattering Lengths of the Polymers and Solvents Studied

Component	**Scattering Length (x 10^{-6} m)**
PEO block	0.636
PCL block	0.847
D_2O	6.37
THF_{d8}	6.35

3.2.1 Pedersen Micelle Model

In order to extract relevant structural parameters from the SANS data, robust models of the scattering intensity as a function of wavevector q are used.[29] The Pedersen model describes a spherical micelle assembly containing a homogeneous spherical core and corona containing Gaussian chains.[10,21,30,31] The form factor model has four main contributing terms: the self-correlation of the core, the self-correlation of the corona, the cross-correlation between the core and the corona, and the self-correlation of the Gaussian corona chains,

$$\begin{aligned} P_{mic}(q) = {} & N_{agg}^2 \beta_{core}^2 A_{core}^2(q) + N\beta_{corona}^2 P_{chain}(q) \\ & + 2N_{agg} N \beta_{core} \beta_{corona} A_{core} A_{corona}(q) \\ & + N_{agg}\left(N_{agg} - 1\right)\beta_{corona}^2 A_{corona}^2(q), \end{aligned} \tag{3.8}$$

$$\text{where } \beta_{core} = v_{core}(\rho_{core} - \rho_{solvent}), \text{and} \tag{3.9}$$

$$\beta_{corona} = v_{PEO}(\rho_{PEO} - \rho_{solvent}). \tag{3.10}$$

N_{agg}, the aggregation number, represents the number of block copolymer chains that comprise the micelle., β_{core} and β_{corona} represent the total excess scattering lengths of the core and corona blocks, respectively, and ρ_{PEO} and $\rho_{solvent}$ are the scattering length densities of the corona PEO block and the bulk solvent, respectively. In the case of β_{core}, we accounted for the effect of the presence of solvent (THF_{d8} and D_2O) in the core on the excess scattering length. Therefore, an additional term is included in our version of the micelle model, $f_{solvent}$, where $f_{solvent}$ is the volume fraction of the core that is solvent and $f_{solvent} + f_{PCL} = 1$, where f_{PCL} is

the volume fraction of PCL in the core. β_{core} is then calculated as a function of $f_{solvent}$ using the following relationships:

$$\rho_{core} = f_{solvent}\rho_{solvent} + f_{PCL}\rho_{PCL}, \text{and} \tag{3.11}$$

$$v_{core} = \frac{v_{PCL}}{f_{PCL}} \tag{3.12}$$

where v_{PCL} is the volume of the PCL block itself, and ρ_{PCL} and ρ_{core} are the scattering length densities of the PCL block and micelle core (including PCL andsolvent), respectively.

For the core self-correlation term, the amplitude is defined as follows for a homogeneous spherical core of radius R_{core} and a smoothly decaying surface scattering length density,[32]

$$A_{core}(q) = \phi(qR_{core}) \exp\left(-\frac{q^2\sigma_{int}^2}{2}\right), \tag{3.13}$$

$$\text{where } \phi(qR_{core}) = \frac{3[sin(qR_{core}) - qR_{core}cos(qR_{core})]}{(qR_{core})^3}, \text{and} \tag{3.14}$$

$$R_{core} = (\frac{3}{4\pi}N_{agg}v_{core})^{1/3}. \tag{3.15}$$

$\phi(qR_c)$ is the form factor amplitude of a sphere and the exponential term in A_{core} accounts for a smoothly decaying scattering length density at the core-corona interface. Since R_{core} is written as a function of v_{core}, $f_{solvent}$ is used as a fitting parameter instead of R_{core},. R_{core} is then calculated directly from the value of $f_{solvent}$ obtained from the fit. In this manner, the effect of solvent swelling the core (which

affects both R_{core} and β_{core}) is accounted for without increasing the number of fitting parameters.

The self-correlation of the PEO chains (treated as Gaussian chains with radius of gyration R_g) in the corona was calculated using the Debye function:

$$P_{chain}(q) = 2\left[\frac{\exp\left(-q^2R_g^2\right) - 1 + q^2R_g^2}{q^4R_g^4}\right] \tag{3.16}$$

where A_{corona} is the scattering amplitude for the corona self-correlation term, and it assumes the PEO corona chains have a radial density distribution $\rho_{chain}(r)$. As the distance from the core-corona interface increases, the density of the chains decreases following this distribution, which is represented in the Pedersen model as a linear combination of two cubic b splines:

$$A_{corona}(q) = \frac{4\pi \int \rho_{chain}(r)[\frac{\sin(qr)}{qr}]r^2dr}{4\pi \int \rho_{chain}(r)r^2dr} \exp\left(\frac{-q^2\sigma_{int}^2}{2}\right) \tag{3.17}$$

$$\rho_{chain}(r) = \frac{\rho_1(r) + a_1\rho_2(r)}{1 + a_1} \tag{3.18}$$

For $R_{core} \le r \le R_{core} + s$,

$$\rho_1(r) = \frac{4(r - R_{core} - s)^3 - (r - R_{core} - 2s)^3}{4s^3}, \text{and} \tag{3.19}$$

$$\rho_2(r) = \frac{-(r - R_{core} - s)^3}{4s^3}. \tag{3.20}$$

For $R_{core} + s \leq r < R_{core} + 2s$,

$$\rho_1(r) = \frac{-(r - R_{core} - 2s)^3}{4s^3}, \text{and} \tag{3.21}$$

$$\rho_2(r) = 0.$$

Elsewhere,

$$\rho_1(r) = 0, \text{and}$$

$$\rho_2(r) = 0.$$

The parameter *s*, shown in Figure 3.1, describes the width of the radial density profile $\rho_{chain}(r)$, while a_1 is the weighting factor for the linear combination of the two splines. σ_{int} is the width of the core-corona interface. These three parameters are all fit and output in the micelle model.

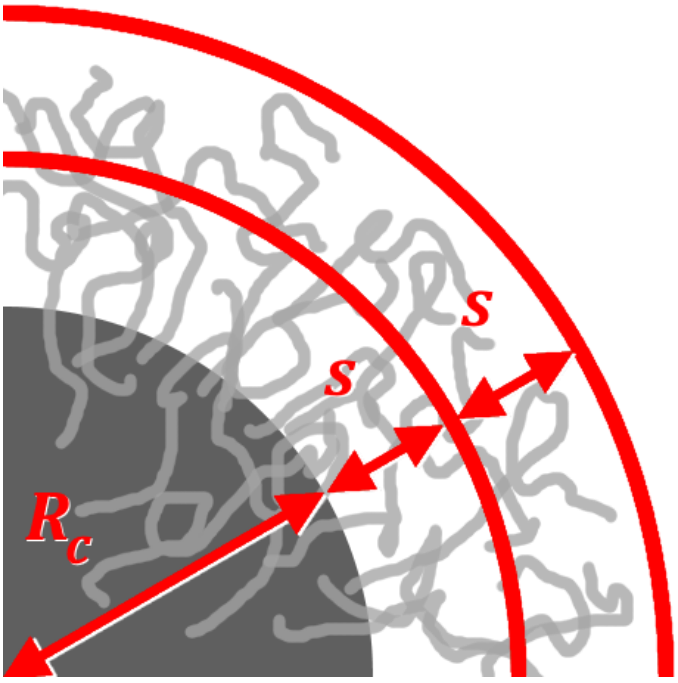

Figure 3.1 A visual depiction of *s*, the width of the corona profile.

A_{corona} is the Fourier transform of $\rho_{chain}(r)$:

$$A_{corona}(q) = \frac{[A_1(q) + a_1 A_2(q)]}{(1 + a_1)} exp \frac{(-q^2 {\sigma_{int}}^2)}{2} \tag{3.22}$$

where

$$\begin{aligned} A_1(q) = C_{norm,1} \Bigg[& \frac{24\cos\{q(R+2s)\}}{q^6} + \frac{6(R+2s)\sin\{q(R+2s)\}}{q^5} \\ & - \frac{96\cos\{q(R+s)\}}{q^6} - \frac{24(R+s)\sin\{q(R+s)\}}{q^5} \\ & + \frac{4(q^4 R s^3 + 3q^2 R s + 18)\cos(qR)}{q^6} \\ & - \frac{2\{2q^2 s^3 - 9(R-2s)\}\sin(qR)}{q^5} \Bigg], \text{and} \end{aligned} \tag{3.23}$$

$$C_{norm,1}^{-1} = \frac{s^4(15R^2 + 14RS + 5s^2)}{5}, \tag{3.24}$$

and

$$\begin{aligned} A_2(q) = C_{norm,2} \Bigg[& \frac{96\cos\{q(R+s)\}}{q^6} - \frac{24(R+s)\sin\{q(R+s)\}}{q^5} \\ & + \frac{4\{q^4 R s^3 - 6q^2 s(R-s) - 24\}\cos(qR)}{q^6} \\ & + \frac{4\{q^2 s^2(3R-s) - 6(R-3s)\}\sin(qR)}{q^5} \Bigg], \text{and} \end{aligned} \tag{3.25}$$

$$C_{norm,2}^{-1} = \frac{s^4(15R^2 + 6RS + s^2)}{15}. \tag{3.26}$$

Since N_{agg} describes the number-average of the number of chains per micelle, polydispersity in micelle size needs to be accounted for. In order to fit this, a Schulz distribution for the core radius is incorporated as

$$G(R_{core}) = \frac{R_{core}^{Z}}{\Gamma(Z+1)}\left(\frac{Z+1}{< R_{core} >}\right)^{Z+1} \exp\left[-\frac{(Z+1)R_{core}}{< R_{core} >}\right], \text{where} \quad (3.27)$$

$$Z = \frac{1}{\sigma_{Rc}^{2}} - 1, \quad (3.28)$$

where $<R_{core}>$ is the average core radius and σ_{Rc} is the core radius polydispersity. This polydispersity term is combined with the micelle form factor to obtain the coherent scattering intensity. To further simplify calculations, Gaussian quadrature was used in place of integration. The coherent scattering intensity,

$$I_{coherent}(q) = \int P_{micelle}(q)G(R_c)dR_c, \quad (3.29)$$

is finally added to the incoherent scattering intensity,

$$I(q) = I_{coherent}(q) + I_{incoherent}(q), \quad (3.30)$$

to get the overall scattering intensity.

In order to best fit the SANS data with this model, the equations were written as a Python code and implemented in SASView using the advanced custom model editor. The following fitting parameters were used: N_{agg}, $f_{solvent}$, s, σ_{int}, σ_{Rc}, $I_{incoherent}$, and a_1. Input parameters included the weight concentration of polymer, molecular weights and densities of the PEO and PCL blocks, the radius of gyration R_g of PEO (taken from Kelley et al.),[12] and the known scattering length densities of the PEO and PCL blocks and the solvents used (THF_{d8} and D_2O). Differential evolution, a

robust genetic fitting algorithm, was implemented in SASView to balance computational speed and robustness, and was run until no further changes were measured in χ^2, a measure of the goodness-of-fit. $R_{micelle}$ and H were calculated using the corona density profile, $\rho_{chain}(r)$ and Equation 3.18. $\rho_{chain}(r)$ was rescaled to $\hat{\rho}_{chain}(r)$ through equating the integral over the corona density profile to the total corona volume,

$$N_{agg} * \nu_{corona} = 4\pi \int \hat{\rho}_{chain}(r) r^2 dr. \quad (3.31)$$

The boundary between the corona and bulk solvent (defining H and therefore $R_{micelle}$) was fixed at the value of r at which $\hat{\rho}_{chain}(r) \leq 0.02$, following prior literature.[10,12,13,28] From there, H was calculated as $R_{micelle} - R_{core}$. In this study, the scattering from unimers was not directly observed in either the SANS or DLS data, and therefore the presence of unimers was neglected.

3.2.2 Solvent Swelling

As discussed previously, a key differentiating factor in this study from previous works is the inclusion of the solvent swelling in the core and how that directly affects the neutron scattering length density of the micelle core. There is a significant effect on the scattering length of the core by including the presence of solvent, and in turn, a significant effect on the intensity calculated from the model. Changing ρ_{core} (and therefore β_{core}) in the model results in a significant impact on the other calculated micelle parameters such as N_{agg} and $f_{solvent}$.

In the micelle samples studied here, the solvents used were THF_{d8} and D_2O, which have near-identical SLDs (6.35×10^{-6} Å^{-2} and 6.37×10^{-6} Å^{-2} respectively), and therefore the fitting program is unable to de-convolute the concentrations of the two solvents in the micelle core, and rather identifies the total solvent concentration in the core.

Chapter 4

Results and Discussion

4.1 Micelle Preparation and Characterization with Dynamic Light Scattering

PEO_{2k}-PCL_{3k} and PEO_{5k}-PCL_{8k} block copolymers were synthesized through the ring-opening of ε-caprolactone with a methoxy-PEO macroinitiator (described in Section 2.1) and the polymers characterized are presented in Table 1.1. The C series (containing PEO_{2k}-PCL_{3k}) and D series (containing PEO_{5k}-PCL_{8k}) micelle solutions were prepared through dissolution of each polymer in THF_{d8} overnight, followed by the dropwise addition of D_2O, and subsequent filtering prior to analysis. DLS data were obtained on the micelle solutions, and R_h and D were extracted through fitting the correlation function with the method of cumulants (Section 3.1). A representative fit to the data is shown in Figure 4.1. The resulting R_h and D values are shown in Tables 4.1 and 4.2.

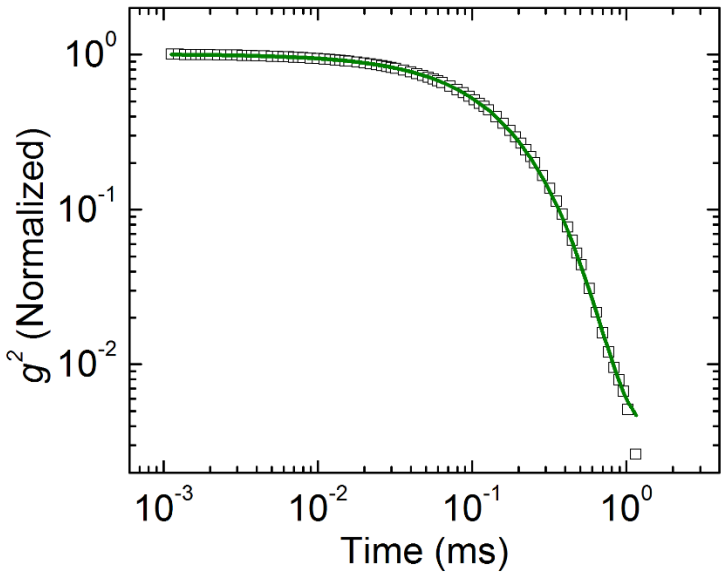

Figure 4.1 Dynamic light scattering data obtained from PEO_{2k}-PCL_{3k} micelles in a solvent mixture containing 30 vol% THF_{d8} (C30). Solid green curve represents the fit using the method of cumulants.

Table 4.1 Dynamic Light Scattering Results for C Series

Sample ID	**Vol% THF_{d8} : Vol% D_2O in Bulk Solvent**	***D* (x 10^{-11} m^2/s)**	**R_h (nm)**
C10	10 : 90	2.48	3.33
C20	20 : 80	2.04	3.42
C30	30 : 70	1.71	3.61
C40	40 : 60	1.47	3.93
C50	50 : 50	1.44	3.68

Table 4.2 Dynamic Light Scattering Results for D Series

Sample ID	Vol% THF_{d8} : Vol% D_2O in Bulk Solvent	D (x 10^{-11} m^2/s)	R_h (nm)
D10	10 : 90	2.17	3.80
D20	20 : 80	1.73	4.04
D30	30 : 70	1.46	4.21
D40	40 : 60	1.28	4.51
D50	50 : 50	1.04	5.09
D60	60 : 40	8.02	6.69

4.2 SANS Data Analysis

As described in Section 3.2, the micelle form factor model includes six structural fitting parameters (N_{agg}, $f_{solvent}$, s, σ_{int}, σ_{Rc}, and a_1), which are extracted from the model. One other fitting parameter is also extracted, $I_{incoherent}$, to describe the incoherent scattering resulting from the bulk solvent. From these seven fitting parameters, the micelle core radius, corona thickness, and overall micelle radius are calculated. Two series of micelle samples were examined: C series (containing PEO_{2k}-PCL_{3k}) and D series (containing PEO_{5k}-PCL_{8k}). In each series, the % THF_{d8} in the bulk solvent was varied from 10-60%.

The scattering intensity as a function of scattering vector q for two representative micelle samples, C20 and D20, are shown in Figure 4.2. The micelle form factor model captures key features of the data, including the low-q plateau, drop off in intensity at intermediate q, and features at intermediate q due to the

presence of the corona. In the following sections, trends in key parameters obtained from the fitting of this model to the data are discussed.

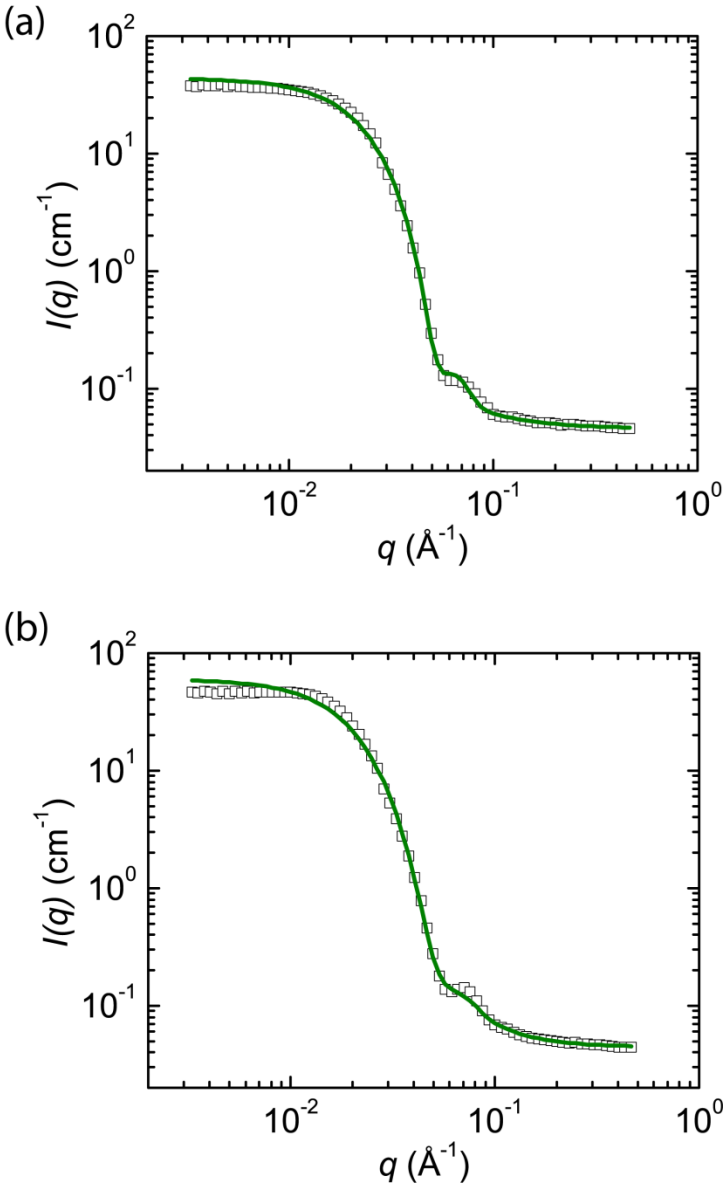

Figure 4.2 Small angle neutron scattering data (open black squares) obtained from (a) C20 and (b) D20 micelle solutions and fit to the micelle form factor model (solid green curve). Error bars represent error on the measurement of scattering intensity and are smaller than the data points in most cases.

4.3 Solvent Swelling of Micelle Core and Impact on Aggregation Number

The aggregation number (N_{agg}) and fraction of the micelle core which is solvent ($f_{solvent}$) are two fitting parameters extracted from the Pedersen micelle model, and are shown in Figure 4.3. The aggregation number defines the number of block copolymer chains in each micelle. The swelling of the micelle core with solvent (D_2O or THF_{d8}) impacts both how the micelle assembles, as well as the scattering profile observed in the SANS experiments. Combined, the volume of the solvent in the core and the volume of PCL in the core (which is taken to be the volume of a single PCL block multiplied by N_{agg}) comprise the entire core volume. Furthermore, the presence of solvent impacts the excess scattering length of the core, which dictates the contrast between the micelle core and bulk solvent. Both of these fitting parameters affect the low q region of the SANS profile primarily, and they have the largest contribution at that scattering vector range.

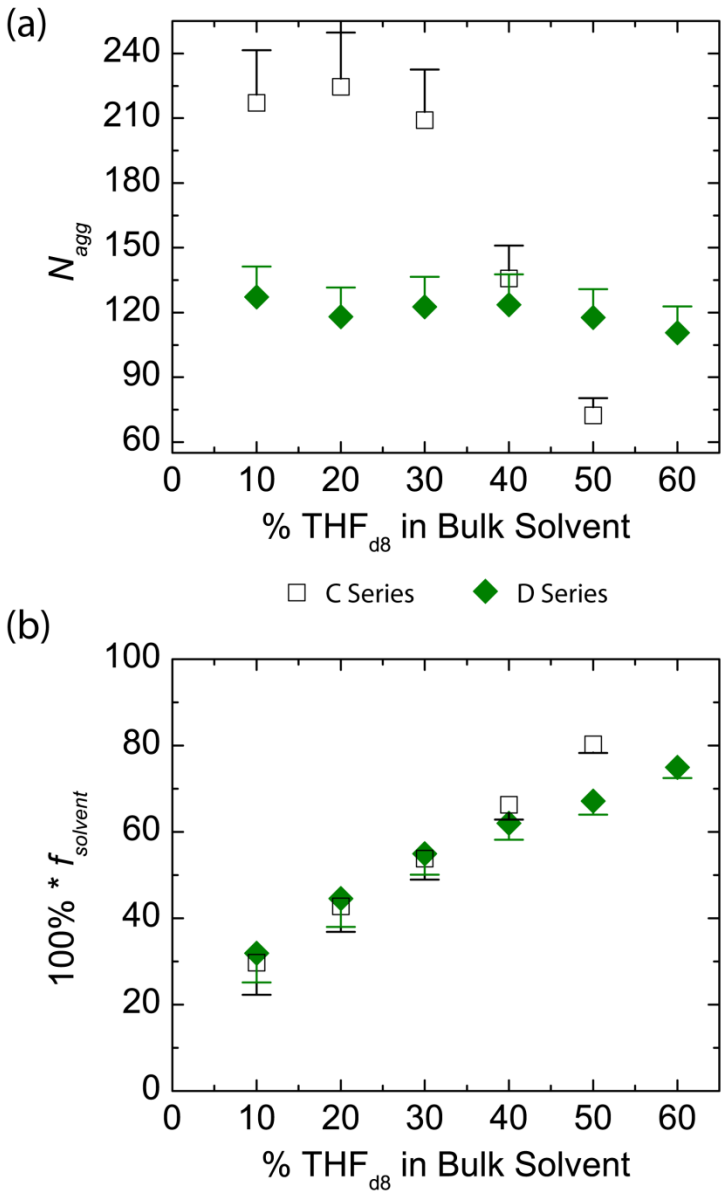

Figure 4.3 (a) Aggregation number (N_{agg}) and (b) solvent volume fraction in micelle core ($f_{solvent}$) as functions of the amount of THF_{d8} in the bulk solvent. Error bars represent the effect of 10% loss in polymer content; error on model fitting is estimated to be smaller than the data point size.

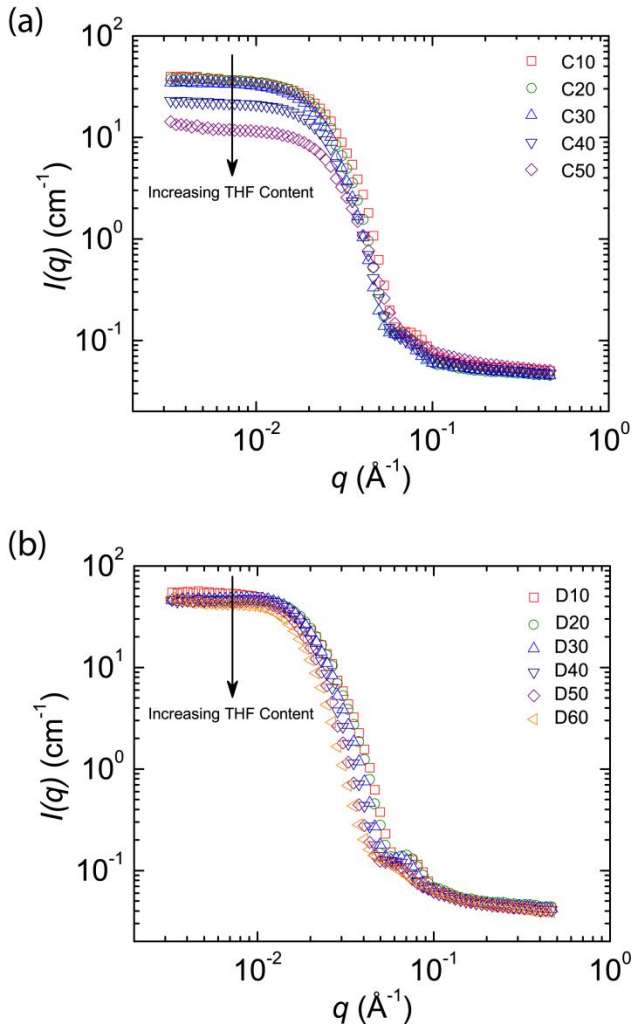

Figure 4.4 Effect of THF_{d8} content in the bulk solvent on the scattering profiles of the (a) C series and (b) D series micelles.

The effect of the decrease in the aggregation number in the C series can be seen when looking at the scattering intensities of all five solvent ratios (Figure 4.4). The low q intensity plateau significantly and systematically decreases with increasing THF_{d8} content. For the D series, in which little change in N_{agg} was observed, the low-q intensity plateau is fairly constant.

4.4 Modeling the Corona Profile

The corona profile width *s* (shown in Figure 4.5), as described earlier in Section 3.2.1, details the corona density profile over which range of *r* (distance from the center of the micelle) each of the two cubic b spline functions ($\rho_1(r)$. and $\rho_2(r)$) contribute and are balanced with the weighting parameter a_1 (Figure 4.1). All of the model fits to the SANS data shown here resulted in a_1 values greater than 10^{10}, in which case the relative importance of $\rho_1(r)$ was negligible. In this case, $\rho_{chain}(r)$ simplifies to simply $\rho_2(r)$. On a related note, *s* is larger than *H* (the corona thickness) for both series at all solvent contents, reinforcing that there is only one spline used in calculating $\rho_{chain}(r)$ (Equations 3.18-3.21). A representative plot of $\hat{\rho}_{chain}(r)$is shown in Figure 4.6, illustrating how the corona thickness (H) is determined from the profile.

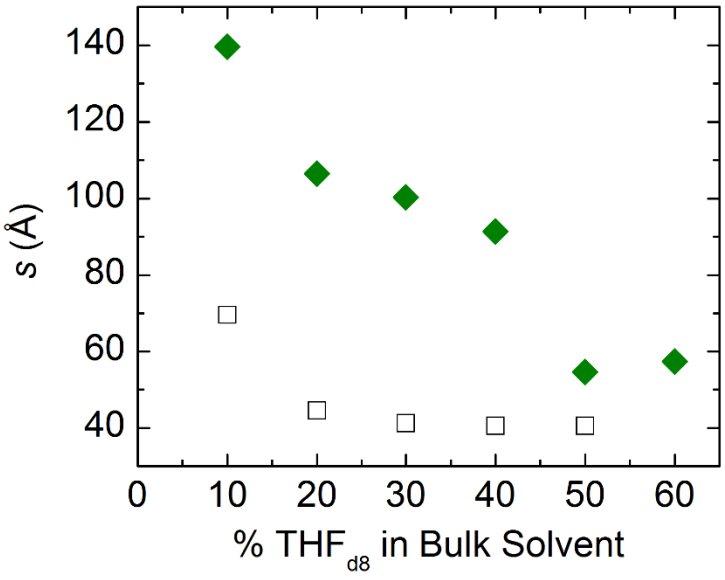

Figure 4.5 Effect of THF_{d8} content in the bulk solvent on the corona profile width, *s*. Error bars were smaller than the data points.

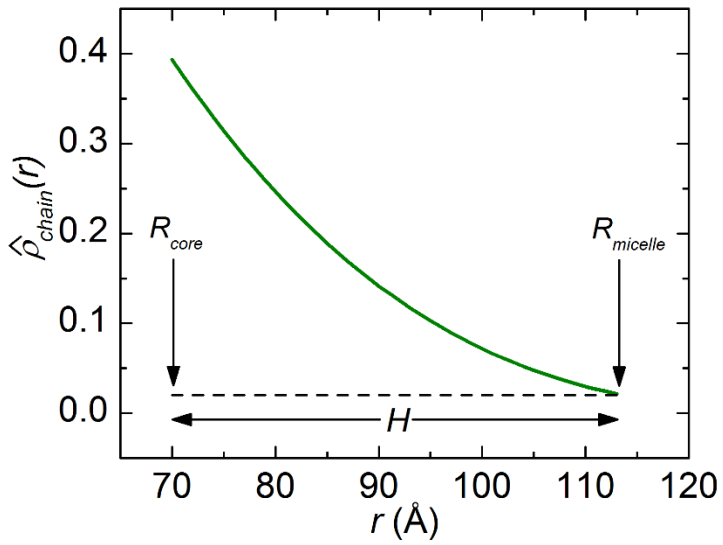

Figure 4.6 Rescaled corona profile $\hat{\rho}_{chain}(r)$ (green solid curve) as a function of *r* for C10. The cutoff value of ρ_{chain} was set to 0.02 (black dashed line) following prior literature, [12,13,31,33] which we have taken to be the outer limit of the corona.

4.5 Effect on Solvent Composition on Core Radius (R_{core}), Corona Thickness (H), and Micelle Radius ($R_{micelle}$)

As discussed earlier in Section 3.2.1, R_{core} is calculated from the volume of the micelle core, which is determined using fitting parameters such as N_{agg} and the amount of solvent that has swelled the core ($f_{solvent}$). The corona thickness, H, is calculated directly from the corona fitting parameters s and a_1, using the corona radial density profile ($\rho_{chain}(r)$). Combining these two results computes the total micelle size, $R_{micelle} = R_{core} + H$. The micelle size parameters are summarized in Figure 4.7 for both the C and D series micelles.

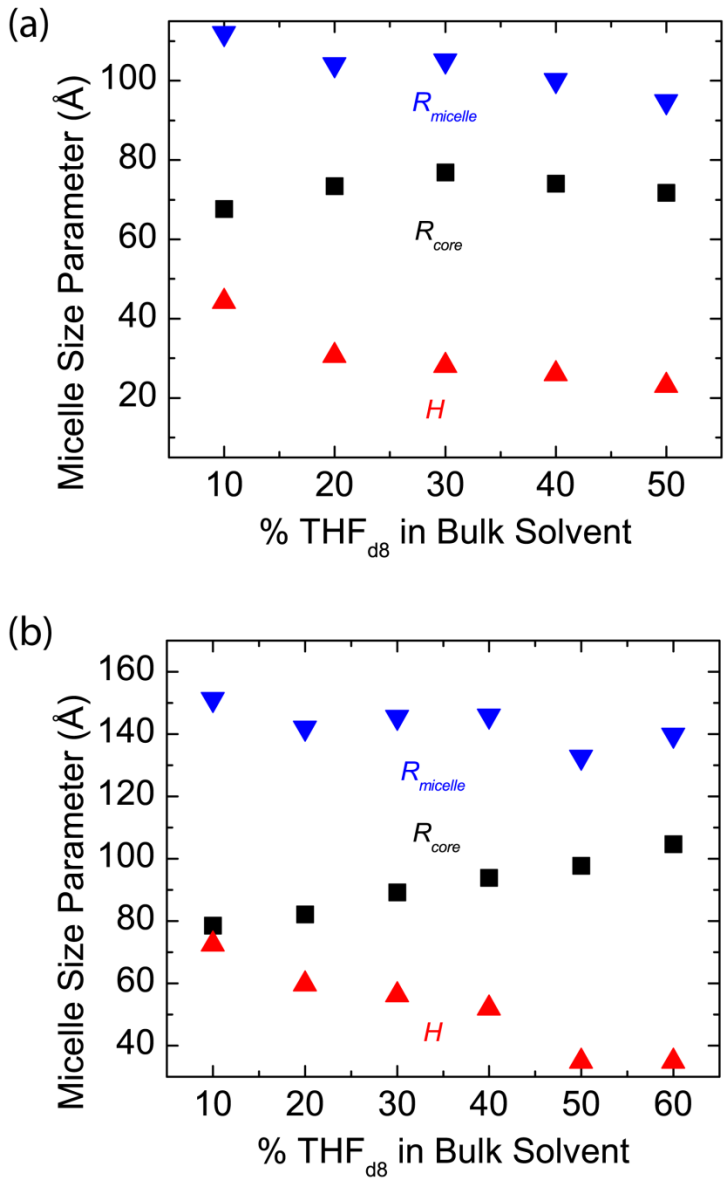

Figure 4.7 Effect of THF_{d8} content in the bulk solvent on the sizes of (a) C series and (b) D series micelles. Error bars are smaller than the data points.

For the lower molecular weight C series, seen in Figure 4.7a, the core radius R_{core} was relatively constant, and exhibited a slight maximum at intermediate THF_{d8} concentrations in the bulk solvent, while the corona thickness H decreased significantly as the THF_{d8} content in the bulk solvent increased. This resulted in an

overall decrease in micelle radius $R_{micelle}$. In the higher molecular weight D series, the increase in R_{core} counteracted the decrease in H, and $R_{micelle}$ was fairly constant.

The trends in R_{core} can be understood by considering trends in N_{agg} and $f_{solvent}$ (core solvent content). For the C series, N_{agg} decreased significantly above 30% THF_{d8} in the bulk solvent, but $f_{solvent}$ linearly increased; the net effect was a relatively constant R_{core}. In the D series, however, N_{agg} was fairly insensitive to the THF_{d8} content in the bulk solvent, while the THF_{d8} content in the core increased, and so R_{core} increased linearly with the THF_{d8} content in the bulk solvent.

4.6 Core-Corona Interfacial Width (σ_{int}) and Core Polydispersity (σ_{Rc})

The core-corona interfacial width (σ_{int}) and core polydispersity ($\sigma_{Rc,}$), as well as s described in the previous section, have the greatest impact on the intermediate q region in the scattering profile (between 0.05 $Å^{-1}$ and 0.2 $Å^{-1}$).

As σ_{int} increases, the once-sharp interface between the core and corona becomes wider and more diffuse. As the % THF_{d8} in the bulk solvent increased, we observed a general trend of increasing $\sigma_{int,}$ with a few anomalous data sets that did not agree with this general trend (Figure 4.8). Prior literature also reported an increase of $\sigma_{int,}$ with increasing co-solvent content.[12] Investigating samples with non-deuterated solvents (and therefore different scattering lengths, for contrast) could help improve the fitting accuracy for σ_{int}.[12]

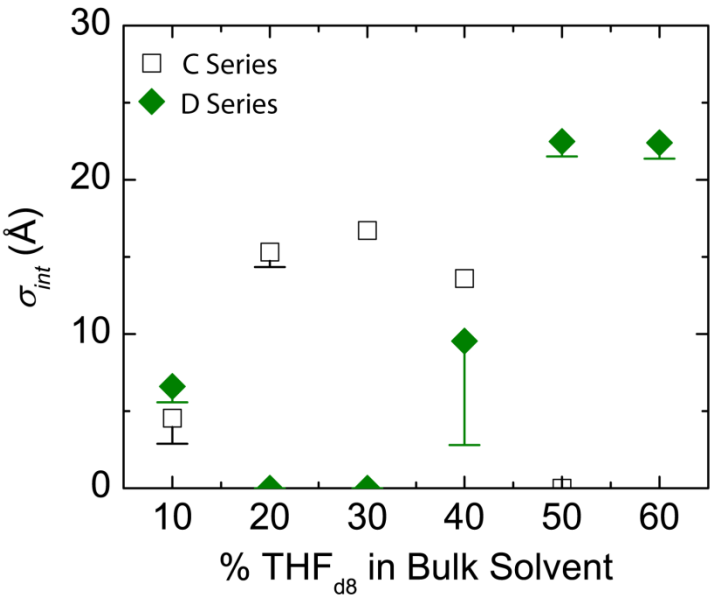

Figure 4.8 Effect of THF_{d8} content in the bulk solvent on σ_{int}. Error bars represent the effect of 10% loss in polymer content; error on model fitting is estimated to be smaller than the data point size.

The core polydispersity (σ_{Rc}) showed differing trends in the C and D series in Figure 4.9. σ_{Rc} increased with increasing THF_{d8} content in the bulk solvent in the C series, and showed the opposite trend in the D series. Notably, the polydispersity of the C series core increased significantly at the THF_{d8} content that the aggregation number decreased rapidly.

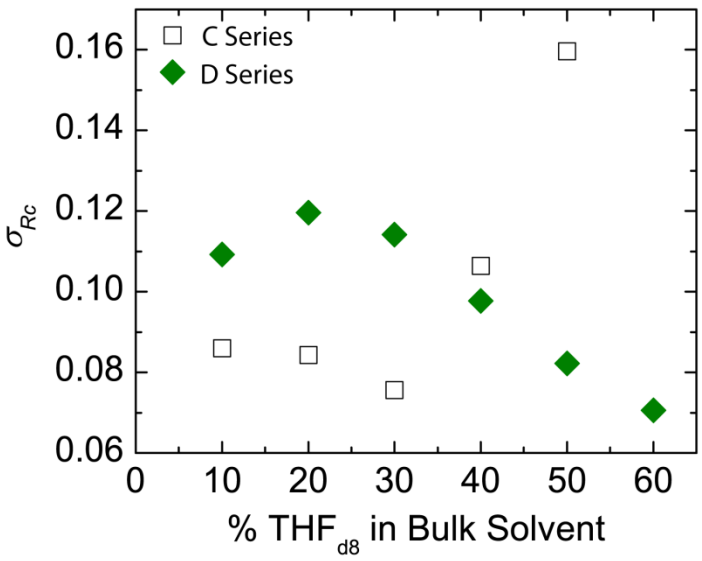

Figure 4.9 Effect of THF_{d8} content in the bulk solvent on σ_{Rc}. Error bars are smaller than the data points.

4.7 Fitting Parameter Correlation

In a complex model such as the micelle form factor model, there are so many different fitting parameters which might be highly correlated (positively or negatively), to the point that they are unnecessary. Using a population-based fitting algorithm known as DREAM, the correlation of any given parameter with every other parameter was investigated for this model.

In Figure 4.10, correlations between the fitting parameters are shown visually: the more isotropic a plot is, the less correlated the corresponding parameters are. For example, N_{agg} is relatively isotropic for most plots, with the exception of the plots showing its correlation with $f_{solvent}$ and s, which are slightly anisotropic and tilted to the left and right, respectively. This means there is a slight negative correlation with $f_{solvent}$, and a small increase in one will result in a minor decrease in the other (as well as slight positive correlation with s). The spline

weighting parameter, a_1, is seen to have bold lines in relation to the other parameters. The fit is therefore not sensitive to that parameter in regards to our system.

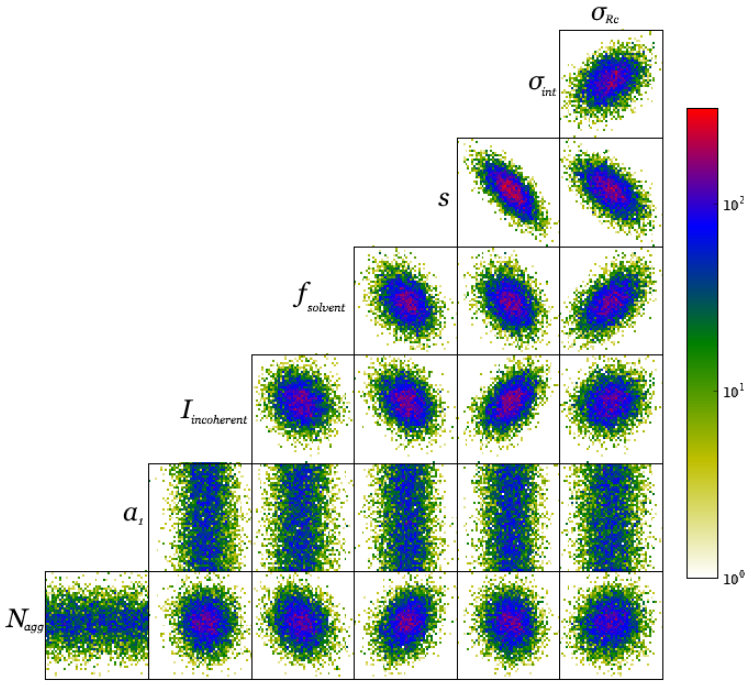

Figure 4.10 Fitting parameter correlation plots, relating how much one parameter affects another.

The anisotropic plots for $f_{solvent}$, s, σ_{int}, and σ_{Rc}, especially with one another, suggest that these particular parameters have significant mutual effects.

4.8 Quantification of Error on Extracted SANS Model Parameters

We considered three main quantifiable sources of error in the SANS experiments and modeling: 1) instrumental error on the measured scattering intensity,[34] 2) error in model fitting to the SANS data, and 3) error in measured polymer mass used in micelle preparation. The wavelength spread of the

instrument has been directly incorporated into the model smearing.[34] The numerical effect of each type of error on fitting results for C10 is quantified in Table 4.3.

Table 4.3 Significance of Sources of Error for C10 Fitting

	N_{agg} Error (%)	$f_{solvent}$ Error (%)	s Error (%)	σ_{int} (%)	σ_{Rc} (%)	I_{inc} (%)
Intensity Error	±0.309	±0.0974	±0.690	±10.3	±0.515	±0.499
Model Fitting	±1.38	±2.02	±2.73	±24.4	±6.98	±2.09
10% Polymer Loss	+11.1	-24.6	+1.44	-37.8	+0.581	-0.420

Table 4.3 Significance of Sources of Error for C10 Fitting (Continued)

	R_c Error (%)	H Error (%)	$R_{micelle}$ Error (%)
Intensity Error	±0.148	±0.680	±0.268
Model Fitting	±0.591	±3.39	±1.70
10% Polymer Loss	+0.295	+2.93	+1.34

The first source of error, instrumental error, is due to the uncertainty in measuring the scattering intensity (error on *I*). The error on *I* is provided during the experiment, and is typically smaller than the data points when *I(q)* is plotted. The effect of error on *I* on the model fitting parameters was quite insignificant, and the error bars are generally smaller than the data points for the plots in Chapter 4 when this class of error is considered.

Error in model fitting was also considered. In order to study how much each parameter affected the goodness-of-fit in the minimization of χ^2, a single parameter was varied from the best-fit results, and the resultant χ^2 recorded. Then, the difference in χ^2 was plotted against the difference in the parameter. Using this, an error threshold (in this case, 2%) was established providing the limits of the parameter within which a similar quality of fit could be obtained. An example of such a plot is shown in Figure 4.11 for N_{agg}. Generally the model fitting errors were also quite small, and in the plots in Chapter 4 the error based on model fitting was established to generally be smaller than the size of the data points. Tables 4.4-4.7 show the effect of the model fitting error on the extracted parameters, represented by italicized text.

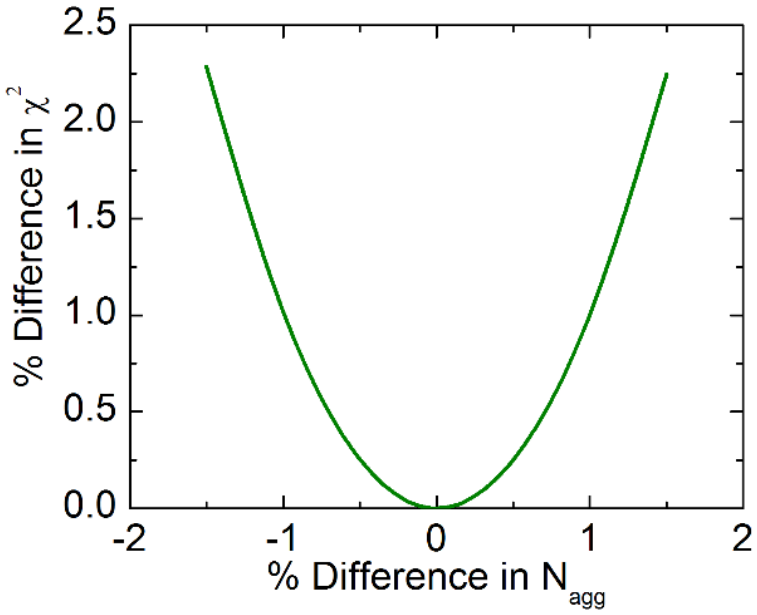

Figure 4.11 Effect of varying N_{agg} on χ^2. A small symmetric distribution gives confidence on the calculation of the parameter.

The final error considered was the error in the total polymer mass that composes the micelles. During micelle synthesis and preparation, there is a small amount of loss of sample, likely due to aggregation and subsequent filtering. . We quantified this loss for select samples and found it to be typically <5% of the total mass. As such, we set a threshold as 10% sample loss in order to probe the impact of the mass loss on the SANS data fitting. The SANS data sets were fit using polymer concentrations of 1 weight percent (no loss) and 0.9 weight percent (10% loss). The error bars in Figures 4.3 and 4.8 indicate uncertainties in the fit parameters due to mass loss of polymer. (In other Figures in Chapter 4, this error was smaller than the size of the data points). With the decrease in total polymer mass, the fitting shows a greater micelle aggregation number, as well as decreased swelling of the micelle core with solvent. The combination of those two factors, however, resulted in little change in the size of the micelles, as seen in Figure 4.7, where the error bars (accounting for polymer loss) were smaller than the data points. Tables 4.4-4.7 show the effect of uncertainty in the sample mass on the extracted model parameters, represented by bold text. Polymer loss was regarded as the most impactful source of error, due to the significant changes in N_{agg} and $f_{solvent}$, as seen in Table 4.3.

4.9 Summary of Micelle Model Fitting to SANS Data

The following tables summarize the extracted fitting parameters and calculated size parameters.

Table 4.4 SANS Model Fitting Parameters Extracted for the C Series†

Sample ID	N_{agg}	$100*f_{solvent}$ (%)	s (Å)	σ_{int} (Å)	σ_{Rc} (Å)
C10	217 *± 3* **(+24)**	29.7 *± 0.6* **(-7.3)**	69.6 *± 1.9* **(+1.0)**	4.5 *± 1.1* **(-1.7)**	0.086 *± 0.006* **(+5e-4)**
C20	225 *± 3* **(+25)**	42.8 *± 0.8* **(-5.9)**	44.6 *± 2.8* **(+3.3)**	15.3 *± 0.5* **(-1.0)**	0.084 *± 0.010* **(+9e-4)**
C30	209 *± 4* **(+23)**	53.8 *± 0. 7* **(-4.8)**	41.2 *± 3.4* **(+0.7)**	16.7 *± 0.6* **(-0.4)**	0.076 *± 0.013* **(+0.002)**
C40	136 *± 2* **(+27)**	66.3 *± 0.5* **(-3.4)**	40.5 *± 3.0* **(+0.9)**	13.6 *± 0.7* **(-0.6)**	0.106 *± 0.010* **(+0.001)**
C50	72 *± 1* **(+15)**	80.3 *± 0.3* **(-2.0)**	40.5 *± 2.1* **(-2.0)**	7e-5 *± --* **(-1e5)**	0.160 *± 0.005* **(-0.001)**

† Italicized text denotes error in model fitting (i.e. within the error, variations in fitting parameters produced fits with comparable least square errors). Bold text denotes error due to a potential maximum 10% loss in polymer mass during sample preparation.

Table 4.5 Parameters Calculated from the Fitting Parameters for the C Series†

Sample ID	R_{core} (Å)	H (Å)	$R_{micelle}$ (Å)
C10	67.7 *± 0.4* **(+0.2)**	44.3 *± 1.5* **(+1.3)**	112.0 *± 1.9* **(+1.5)**
C20	73.4 *± 0.6* **(+0.2)**	30.7 *± 1.7* **(+2.4)**	104.1 *± 2.3* **(+2.6)**
C30	76.9 *± 0.7* **(+0.2)**	28.2 *± 1.3* **(+0.8)**	105.1 *± 2.0* **(+1.0)**
C40	74.0 *± 0.8* **(+0.2)**	26.1 *± 1.1* **(+1.0)**	100.1 *± 1.9* **(+1.2)**
C50	71.7 *± 0.6* **(+0.2)**	23.1 *± 1.1* **(-0.2)**	94.8 *± 1.7* **(+0.0)**

† Italicized text denotes error in model fitting (i.e. within the error, variations in fitting parameters produced fits with comparable least square errors). Bold text denotes error due to a potential maximum 10% loss in polymer mass during sample preparation.

Table 4.6 SANS Model Fitting Parameters Extracted for the D Series†

Sample ID	N_{agg}	$100*f_{solvent}$ (%)	**s (Å)**	**σ_{int} (Å)**	**σ_{Rc} (Å)**
D10	127 *± 2* **(+14)**	31.9 *± 0.6* **(-6.8)**	139.6 *± 3.1* **(-0.4)**	6.6 *± 0.8* **(-1.0)**	0.112 *± 0.005* **(+0.003)**
D20	118 *± 3* **(+13)**	44.6 *± 0.9* **(-6.5)**	106.5 *± 5.1* **(+1.3)**	2.6e-5 *± --* **(1e-7)**	0.120 *± 0.008* **(+3e-4)**
D30	123 *± 3* **(+14)**	54.9 *± 0.8* **(-4.9)**	100.3 *± 5.7* **(-0.9)**	1.3e-5 *± --* **(-6e-6)**	0.114 *± 0.009* **(+0.002)**
D40	124 *± 3* **(+14)**	62.0 *± 0.8* **(-3.8)**	91.3 *± 5.7* **(+7.7)**	9.5 *± 2.1* **(-6.7)**	0.0977 *± 0.011* **(-8e-4)**
D50	118 *± 3* **(+13)**	67.2 *± 0.8* **(-3.2)**	54.6 *± 6.1* **(+1.6)**	22.5 *± 1.1* **(-1.0)**	0.0852 *± 0.018* **(+0.003)**
D60	111 *± 3* **(+12)**	74.9 *± 0.5* **(-2.4)**	57.3 *± 5.6* **(-1.4)**	22.4 *± 1.0* **(-1.0)**	0.0742 *± 0.018* **(+0.004)**

† Italicized text denotes error in model fitting (i.e. within the error, variations in fitting parameters produced fits with comparable least square errors). Bold text denotes error due to a potential maximum 10% loss in polymer mass during sample preparation.

Table 4.7 Parameters Calculated from the Fitting Parameters for the D Series†

Sample ID	R_{core} (Å)	H (Å)	$R_{micelle}$ (Å)
D10	78.6 *± 0.5* **(+0.3)**	72.6 *± 1.5* **(+1.8)**	151.2 *± 2.0* **(+2.1)**
D20	82.2 *± 1.0* **(-0.1)**	59.8 *± 2.0* **(+2.2)**	142.0 *± 3.0* **(+2.1)**
D30	89.2 *± 1.3* **(+0.1)**	56.3 *± 1.8* **(+1.1)**	145.5 *± 3.1* **(+1.2)**
D40	95.0 *± 1.4* **(+1.1)**	52.0 *± 1.7* **(+4.1)**	145.9 *± 3.1* **(+5.2)**
D50	97.7 *± 1.6* **(+0.4)**	35.0 *± 3.0* **(+1.5)**	132.7 *± 4.6* **(+1.9)**
D60	104.7 *± 1.5* **(+0.5)**	35.0 *± 1.9* **(+1.3)**	139.7 *± 3.4* **(+1.8)**

† Italicized text denotes error in model fitting (i.e. within the error, variations in fitting parameters produced fits with comparable least square errors). Bold text denotes error due to a potential maximum 10% loss in polymer mass during sample preparation.

Chapter 5

Conclusions

Micelle assembly characteristics were probed through variation of both solvent composition (ratio of D_2O to THF_{d8}) and polymer molecular weight. The combined use of DLS and SANS allowed for detailed structural information to be extracted. The inclusion of THF_{d8} and D_2O swelling in the core in the micelle SANS model fitting improved the accuracy and robustness of the fits.

As the THF-to-D_2O ratio in the bulk solvent increased, both micelle series showed a linear increase in the THF_{d8} content in the core. Surprisingly, there were significantly different impacts of the THF_{d8} content on other micelle structural parameters. In the low molecular weight C series, the aggregation number decreased rapidly with increasing THF_{d8} content in the bulk solvent, resulting in a relatively insensitive core radius size with THF_{d8} content (as the decrease in aggregation number was offset by swelling of the core with solvent). The corona and overall micelle sizes slightly decreased with increasing THF_{d8} content. In the case of the larger molecular weight D series, the aggregation number was insensitive to the THF_{d8} content in the bulk solvent, and the swelling of the core with solvent resulted in an increase in core radius. This increase in core radius was offset by a decrease in corona thickness, resulting in a constant overall micelle size.

Looking forward, investigating other solvent mixtures (e.g. non-deuterated THF, mixtures of THF and THF_{d8}) and polymer compositions (e.g. molecular weights,

extents of deuteration) would allow for much more robust descriptions of the PEO-PCL micelle parameters and better quantification of how much of a given solvent penetrates the micelle core. Past that, analysis of the ability of the system to encapsulate guest species (drugs, small molecules, nanoparticulates, etc.) should reveal the viability of the PEO-PCL micelles in particular for the many potential applications of these tunable assemblies.

References

(1) Miyata, K.; Christie, R. J.; Kataoka, K. *Reactive & Functional Polymers* **2011**, *71*, 227.

(2) Otsuka, H.; Nagasaki, Y.; Kataoka, K. *Current Opinion in Colloid & Interface Science* **2001**, *6*, 3.

(3) Yang, L.; Alexandridis, P. *Current Opinion in Colloid & Interface Science* **2000**, *5*, 132.

(4) Stubenrauch, K.; Moitzi, C.; Fritz, G.; Glatter, O.; Trimmel, G.; Stelzer, F. *Macromolecules* **2006**, *39*, 5865.

(5) Manet, S.; Lecchi, A.; Imperor-Clerc, M.; Zholobenko, V.; Durand, D.; Oliviera, C. L. P.; Pedersen, J. S.; Grillo, I.; Meneau, F.; Rochas, C. *J. Phys. Chem. B* **2011**, *115*, 11318.

(6) Bang, J.; Jain, S.; Li, Z.; Lodge, T. P. *Macromolecules* **2006**, *39*, 1199.

(7) Bermudez, H.; Brannan, A. K.; Hammer, D. A.; Bates, F. S.; Discher, D. E. *Macromolecules* **2002**, *35*, 8203.

(8) Yang, L.; Alexandridis, P. *Macromolecules* **2000**, *33*, 5574.

(9) Zhang, L.; Eisenberg, A. *Macromolecules* **1999**, *32*, 2239.

(10) Pedersen, J. S.; Gerstenberg, M. C. *Colloids and Surfaces A: Physicochemical and Engineering Aspects* **2003**, *213*, 175.

(11) Lund, R.; Willner, L.; Stellbrink, J.; Radulescu, A.; Richter, D. *Macromolecules* **2004**, *37*, 9984.

(12) Kelley, E. G.; Smart, T. P.; Jackson, A. J.; Sullivan, M. O.; III, T. H. E. *Soft Matter* **2011**, *7*, 7094.

(13) Bang, J.; Viswanathan, K.; Lodge, T. P.; Park, M. J.; Char, K. *J. Chem. Phys.* **2004**, *121*, 11489.

(14) Mortensen, K.; Pedersen, J. S. *Macromolecules* **1993**, *26*, 805.

(15) Yang, L.; Alexandridis, P. *Langmuir* **2000**, *16*, 4819.

(16) Choi, S.-H.; Bates, F. S.; Lodge, T. P. *J. Phys. Chem. B* **2009**, *113*, 13840.

(17) Lohmeijer, B. G. G.; Pratt, R. C.; Leibfarth, F.; Logan, J. W.; Long, D. A.; Dove, A. P.; Nederberg, F.; Choi, J.; Wade, C.; Waymouth, R. M.; Hedrick, J. L. *Macromolecules* **2006**, *39*, 8574.

(18) Pratt, R. C.; Lohmeijer, B. G. G.; Long, D. A.; Waymouth, R. M.; Hedrick, J. L. *J. Am. Chem. Soc.* **2006**, *128*, 4556.

(19) Taniewska-Osińska, S.; Nowicka, B.; Kacperska, A.; Bald, A. *Physics and Chemistry of Liquids* **1993**, *25*, 113.

(20) Kline, S. R. *J. Appl. Cryst.* **2006**, *39*, 895.

(21) Pedersen, J. S. *J. Appl. Cryst.* **2000**, *33*, 637.

(22) Frisken, B. J. *Applied Optics* **2001**, *40*, 4087.

(23) Provencher, S. W. *Computer Physics Communications* **1982**, *27*, 229.

(24) Li, Y.; Lubchenko, V.; Vekilov, P. G. *Rev. Sci. Instrum.* **2011**, *82*.

(25) Pusey, P. N.; Koppel, D. E.; Schaefer, D. E.; Camerini-Otero, R. D.; Koenig, S. H. *Biochemistry* **1974**, *13*, 952.

(26) Koppel, D. E. *J. Chem. Phys.* **1972**, *57*.

(27) Jackson, A. J.; Research, N. C. f. N., Ed. Gaithersburg, MD, 2008.

(28) Castelletto, V.; Hamley, I. W. *Current Opinion in Colloid & Interface Science* **2002**, *7*, 167.

(29) Mildner, D. F. R.; Carpenter, J. M. *J. Appl. Cryst.* **1984**, *17*, 249.

(30) Pedersen, J. S.; Svaneborg, C. *Current Opinion in Colloid & Interface Science* **2002**, *7*, 158.
(31) Pedersen, J. S.; Svaneborg, C.; Almdal, K.; Hamley, I. W.; Young, R. N. *Macromolecules* **2003**, *36*, 416.
(32) Smirnov, A. V.; Deryabin, I. N.; Fedorov, B. A. *Journal of Applied Crystallography* **2015**, *48*, 1089.
(33) Castelletto, V.; Hamley, I. W.; Pedersen, J. S. *The Journal of Chemical Physics* **2002**, *117*.
(34) Barker, J. G.; Pedersen, J. S. *J. Appl. Cryst.* **1995**, *28*, 105.